FEATURES OF THE INTERACTION AND FORMATION OF NANOSTRUCTURED CHITOSAN SYSTEMS DURING IONOTROPIC GELATION

Rakiya Yunusovna Milusheva[1,a], Ilnar Nakipovich Nurgaliev[1,b,*], Sayora Sharafovna Rashidova[1,c]

[1] – Institute of Chemistry and Physics of Polymers of Scientific Academy of Uzbekistan, Tashkent 100128, Uzbekistan
[a] – ORCID: 0000-0003-2573-1013, [b] – ORCID: 0000-0002-6983-4375,
[c] – ORCID: 0000-0003-3104-6004
[*]corresponding author: ilnarvodnik@gmail.com

Abstract

Bombyx mori chitosan nanoparticles (ChS NPs) were obtained and the kinetic aspects of their size distribution depending on the degree of nonequilibrium of the synthesis by ionotropic gelation using sodium tripolyphosphate (TPP) were studied. The size of ChS NPs was greatly influenced by the ChS concentration, which varied from 0.5 to 10 mg/ml. The size of the NPs increased from 100 to 300 nm when the ChS concentration increased from 0.5 to 10 mg/ml and while maintaining all other parameters of the reaction. An increase in the ChS to-TPP ratio corresponded to a lower cross-linking density and thus ensured slower kinetics for NP formation alongside the formation of large chitosan/TPP aggregates. There was an almost threefold increase in the particle size when the pH of the medium increased from 3.8 to 4.7; thus, the size of ChS NPs depends on the pH of the solution. There was a slight agglomeration of NPs from 363 to 642 nm with an increase in the NP synthesis time from 4 to 24 h. According to calculations, the maximum interaction energy is 50.4 and 69.4 kcal/mol for deprotonated TPP ($P_3O_{10}^{5-}$); after adiabatic transfer of the proton, the value decreases to 32.9–33.5 kcal/mol. The maximum interaction energy is –12.8 kcal/mol for the initially protonated TPP ($H_4P_3O_{10}^{-}$).

Keywords: *Bombyx mori chitosan, tripolyphosphate, nanoparticles, ionic gelation, modelling, interaction energy*

Received: 11.12.2023
Accepted: 16.05.2024

1. Introduction

There is extensive research on chitosan-based nanoparticles (ChS NPs), especially for the design and development of new drug-delivery systems. These NPs have numerous beneficial properties such as biocompatibility, biodegradability, bioactivity, mucoadhesion and hydrophilicity, which facilitate the administration of poorly absorbed drugs through various epithelial barriers such as the cornea and the nasal and intestinal mucosa [1]. These systems can be produced under aqueous and fairly mild conditions to preserve the bioactive conformation of sensitive macromolecules (e.g. hormones, antigens, DNA and growth factors) that would otherwise be susceptible to enzymatic degradation and hydrolysis [2, 3]. Usually, ChS NPs are formed according to a 'bottom-up' approach as a result of self-assembly or stitching in which molecules are arranged into ordered nanoscale structures due to physical, covalent inter- or intramolecular interactions. A recognised feature of these nanosystems is their ability to protect hydrophilic macromolecules from degradation and to overcome mucosal barriers. One of the ways to create ChS NPs using self-assembly is ionotropic gelation using sodium tripolyphosphate (TPP), which is non-toxic.

ChS is one of the most popular components in the creation of NPs for the delivery of drugs. However, the ability to reproduce ChS NPs consistently is often a problem; therefore, great attention is paid to the purity and accurate characterisation of the source material and to the development of preparatory procedures. The processes used to obtain ChS NPs via ionotropic gelation are quite well known, but the influence of various factors on the particle size requires further investigation. Ionotropic gelation of ChS NPs involves the use of ionic cross-linking agents [4]. When TPP is used as an ionic cross-linking agent, two aqueous phases – one containing ChS and another containing polyanionic TPP – are mixed to form a complex coacervate [5]. The CS/TPP molar ratio and the developed interactions are crucial to ensure NPs exhibit the appropriate size, which can affect the drug release properties. However, the mechanism by which ChS and TPP interact has not been well documented in the literature. It has been suggested that all ionic groups of TPP can participate in interactions with ChS amine groups. However, an oversimplified model of interaction sites lacks accuracy and, to the best of our knowledge, this issue has yet to be addressed.

Electrostatic interactions between the cationic amino groups of ChS and the negatively charged anions of the cross-linker promote the formation of NPs. The size and surface charge of particles can be modified by changing the ratio of ChS and stabiliser [6]. Attempts have been made to optimise the processing parameters of ChS in the process of ionic gelation [7], but there are no unambiguous systematic conclusions in this area of research.

Most research in the field of synthesis of CS NPs is related to raw materials from armoured crustaceans. There has been limited investigation regarding the preparation and specific features of the formation of ChS NPs obtained from the pupae of the silkworm *Bombyx mori*. The present work aimed to generate *B. mori* ChS NPs using ionotropic gelation. Subsequently, the influence of various parameters on the size of the NPs was assessed. We also performed theoretical analysis: we elucidated the aspects of the ChS and TPP interactions, calculated the interaction energy, identified interaction sites and located energetically favourable relative configurations. Of note, the structure of a polymer and its spatial configuration in real experimental conditions depend on numerous factors such as the number of monomers, pH, the ionic strength of the environment, temperature, the solvent type and inter- and intra-molecular interactions such as hydrogen bonding, among others. It is practically impossible to simulate such conditions, especially using quantum methods. For this endeavour, we chose to limit the study to the interactions between a ChS pentamer and two types of TPP anions.

2. Materials and Methods

2.1. Obtaining *Bombyx mori* Chitosan Nanoparticles

Purified *B. mori* ChS was dissolved in 2% acetic acid at a concentration of 0.5 mg/ml. A TPP solution (1 mg/ml) was prepared in distilled water. Both solutions were filtered through filters with a pore size of 0.22 μm. Complexation was carried out by adding the TPP solution dropwise to the ChS solution at 25°C with stirring for 20 min on an MS-PA magnetic stirrer (~300 rpm) (HCS Scientific & Chemical Pte Ltd, Singapore). Then, the mixture underwent treatment in an ultrasonic cleaner FSF 020S (FAITHFUL Instrument, China) at a power of 120 W and a frequency of 40 kHz for 2 min immediately before atomic force microscopy (AFM). The NPs were separated from the working solution by centrifugation (7000 rpm) and freeze-dried at –50 to –55°C and 0.4–0.5 mbar for 3–4 h.

2.2. Determination of the Molecular Weight of Chitosan

The molecular weight of ChS was determined by the viscometric method at 25°C. A 0.5% ChS solution in 0.33 M acetate buffer (pH 4.5) was prepared to determine the viscosity (η). The molecular weight was calculated using the Mark–Kuhn–Houwink equation:

$$M\eta = ([\eta]/K)^{1/\alpha}, \quad (1)$$

where K and α are constants for the given polymer-solvent system at $K = 1.4 \times 10^{-4}$ and $\alpha = 0.83$ [8].

2.3. Determination of the Degree of Deacetylation

The degree of deacetylation (DDA) of the ChS samples was determined by conductometric titration on an analytical instrument (Mettler-Toledo, Switzerland) using a 0.1 M sodium hydroxide (NaOH) solution as a titrant for a ChS solution dissolved in 0.1 M hydrochloric acid (HCl). The amount of alkali required to titrate the acid associated with the amino groups was determined from a graph of the dependence of the electrical conductivity of the solution on the volume of alkali. The degree of deacetylation was calculated using equation (2) [9]:

$$\text{Degree of deacetylation} = [(203 \times N_{NH2})/(1400 + 42\, N_{NH2})] \times 100\%, \quad (2)$$

where N_{NH2} is the amine nitrogen content, calculated as $NH_2 = \Delta V \times C_{NaOH}/m$, where ΔV is the volume of the NaOH solution used for titration of amino groups [ml], C_{NaOH} is the exact concentration of the NaOH solution [mol/l] and m is mass of ChS in the sample [g].

2.4. Determination of the Ash Content

The ash mass fraction was determined using a published procedure [10]. The ash content of the sample (Z) was calculated using equation (3):

$$Z\,(\%) = m \times 100/g, \quad (3)$$

where m is the residual mass after combustion [g] and g is the sample weight [g].

2.5. Determination of Solubility

To determine the solubility of ChS, a specific amount of sample was weighed (0.1–0.5 g) and placed into a glass flask. Then, 2% acetic acid (100 ml) was added, and the mixture was stirred until the ChS was dissolved completely. The working solution was filtered through a Schott filter and dried at 104°C for 2 h. Solubility (P) was determined using equation (4):

$$P\,(\%) = [(g - m)/g] \times 100, \quad (4)$$

where g is the sample weight [g] and m is the amount of substance on the filter [g].

2.6. Fourier-Transform Infrared Spectroscopy

An 'Inventio-S' Fourier-transform infrared (FTIR) spectrometer (Bruker, Germany) was used to measure the spectra of all reaction products in the range of 4000–400 cm^{-1}, because the absorption bands of almost all the functional groups of organic molecules lie in this spectral range. The samples were prepared in the form of tablets with potassium bromide at a pressure of 7×10^8 Pa.

2.7. Determination of the Degree of Crystallinity

X-ray diffraction of the samples were carried out on a Miniflex 600 diffractometer (Rigaku, Japan) with monochromatic CuKα radiation. The samples were examined in the form of compressed pellets. Scanning was carried out in the 2θ range of 10–35°. The degree of crystallinity was calculated using equation (5):

$$\text{Degree of crystallinity (\%)} = [(Ic - Ia)/Ic] \times 100\%, \quad (5)$$

where Ic and Ia are the intensities of crystal reflection and amorphous scattering, respectively [11].

2.8. Total Nitrogen Content

The nitrogen content in the ChS samples was determined using the Dumas gasometric method by combusting a weighed sample (5–10 mg) in a quartz tube under carbon dioxide (CO_2) flow and measuring the volume of liberated nitrogen. The nitrogen content in the sample was calculated using equation (6) [12]:

$$N = [m \times (V - V') \times 100]/g, \quad (6)$$

where m is the mass of 1 ml of nitrogen at a given temperature and pressure; V is the volume of liberated nitrogen [ml], V′ is the correction for a given volume, taking into account the calibration of the gasometer [mL], and g is the weight sample [mg].

2.9. Atomic Force Microscopy

The surface morphology of the samples was analysed by AFM using an Agilent 5500 instrument (USA). Scanning was carried out at room temperature in semi-contact mode in air. Silicon cantilevers with a rigidity of 9.5 N/m and a frequency of 145 kHz were used. The maximum scanning area was 11 × 11 μm^2 in the direction of the X, Y coordinates, and 1 μm in the direction of the Z coordinate. The average NP size and coefficient of variation were determined by processing the corresponding images of the sample surface using the Pico image basic software.

The most common method for producing ChS NPs is the ionotropic gelation of ChS with the non-toxic TPP, a small ion with a triple negative charge over the entire pH range [13–15].

2.10. Computational Methods

Geometry was optimised based on all-electron density functional theory (DFT) calculations. The generalised gradient was approximated with the standard 6-31++G (d,p) basis set [16] and the GAUSSIAN 09 software package. Gaussview 5.0.9 was used for visualisation. Fully protonated ChS oligomers were considered, so the overall charge of the ChS pentamers was set to 5e. The interaction energy and maximum interaction energy configurations of ChS with TPP were calculated by scanning the potential energy surface (PES) with respect to different distances and orientations. The PES scans and interaction energy calculations were performed using Grimme's B97-D functional [17], which includes long-range dispersion corrections, with the def-TZVP basis set [18],

which is of triple-ζ quality. Solvation energy was calculated to quantify the reactivity in the aqueous phase using self-consistent field theory and the polarisable continuum model (PCM) [19, 20]. The basis set superposition error (BSSE) was calculated with the counterpoise (CP) method developed by Boys and Bernardi [21]. It requires the keyword CP = N, where N is the number of fragments to be considered (for an A-B system, N = 2) [22, 23].

The first stage of the theoretical calculation was to determine the optimised molecular structures of ChS and TPP. A chain consisting of five monomers was considered to be the structural unit of ChS. The interaction energy ($\Delta E_{interact}$) was calculated using equation (7):

$$\Delta E_{interact} = E_{ChS\text{-}TTP} - (E_{ChS} + E_{TTP}) + E_{BSSE}, \quad (7)$$

where $E_{ChS–TPP}$, E_{ChS} and E_{TPP} are the energy of the system for ChS-TPP, ChS and TPP, respectively. E_{BSSE} is a BSSE that was calculated using the CP method. When a CP correction is applied in combination with a solvent reaction field, any basis functions of the ghost atoms lying outside the reaction-field cavity may artificially increase the outlying charge and thus produce erroneous results. Therefore, the interaction energy was computed within the solvation model, the CP method was performed in the gas phase and the interaction energy was subjected to the calculated BSSE corrections.

3. Results and Discussion

3.1. Preparation of Chitosan Nanoparticles

The purity and accurate characterisation of ChS is crucial. ChS is characterised by structural and chemical heterogeneity even after processing under drastic chemical conditions and contains a small amount of mineral and protein impurities, so it is necessary to pay attention to its purification.

Generation of *B. mori* ChS NPs required several steps. First, the technical ChS was pre-dissolved in 2% acetic acid, deposited and coagulated at a certain pH, washed in alcohol, centrifuged and lyophilised [24]. Then, it was subjected to elemental analysis and FTIR spectroscopy. The influence of concentration, the pH of the mediums and the NP synthesis time during the preparation of ChS/TPP NPs was studied to minimise polydispersity in size, to ensure stability and to control the average size of NPs. *B. mori* ChS samples with different molecular weights (No. 1–3, Table 1) – all obtained from a technical sample of ChS – were used to evaluate the production of ChS NPs via ionotropic gelation.

Table 1. Physicochemical characteristics of the Bombyx mori chitosan (ChS) samples.

No.	Sample	Cleaning time [h]	N [%]	Z [%]	P [%]	Mη [kDa]	DDA [%]	DC [%]
0	ChS technical	–	7.83	7.17	85.56	194	52.2	40
1	ChS purified-1	6	7.20	1.43	96.7	130	85.8	25
2	ChS purified-2	4	8.32	0.44	99.85	152	96.5	32
3	ChS purified-3	2	8.10	0.79	98.36	165	94.4	30

Note. Abbreviations: DC, degree of crystallinity; DDA, degree of deacetylation; Mη, molecular weight; P, solubility; N, nitrogen content; Z, ash content.

The molecular weight of technical *B. mori* ChS, determined by the viscometric method, was 194 kDa (Table 1). When purified, the molecular weight decreased slightly to 130–165 kDa and the degree of deacetylation increased from 52.2% to 85.8%–96.5%. As the degree of deacetylation increased, the solubility of the samples increased from 85.56% to 99.85%. This increased solubility is due to a reduction in the number of acetamide groups of chitin as they are converted into amino groups [25]. Thus, during purification, ChS becomes more structurally homogenous.

As mentioned above, the molecular weight of ChS was determined by the viscometric method (Figure 1). Intrinsic viscosity was calculated using the Huggins equation (top line) and the Kremer equation (bottom line). Their applicability is due to the preservation of the linear dependence of the reduced viscosity on the polymer concentration in solution and the absence of strong intermolecular interactions between the macrochain units.

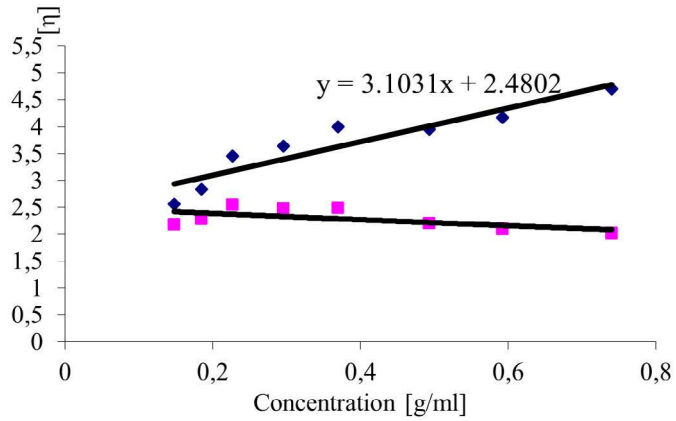

Figure 1. Determination of the molecular weight of sample No. 1 (see Table 1) by the viscometric method: [η] = 2.48 dl/g, [η] = 1.40×10^{-4} and Mη = 130 kDa.

The degree of deacetylation of sample No. 1 (see Table 1) was determined with conductometric titration. It was 85.8% (Figure 2).

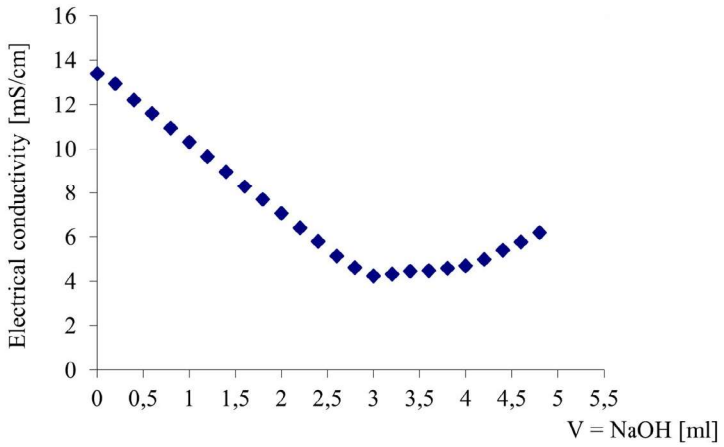

Figure 2. Conductometric titration of sample No. 1 (see Table 1): Mη = 130 kDa and degree of deacetylation = 85.8%.

Sample No.1 was also evaluated with FTIR spectroscopy (Figure 3). The intense broad band at 3500–3100 cm^{-1} indicates absorption of –OH and $–NH_2$ groups included in hydrogen bonds. There are stretching vibrations of –CH and $–CH_2$ groups at 2920 and 2980 cm^{-1}, respectively. There is almost complete absence of an absorption band at 1640 cm^{-1} (amide I) and an intense absorption band at 1579 cm^{-1}, corresponding to the angular deformation of the $–NH_2$ (amide II). These changes indicate effective purification of the original (technical) ChS. Absorption bands in the range of 900–1150 cm^{-1} are from various deformation vibrations of =C-O-C=, –NH and =C-C= groups.

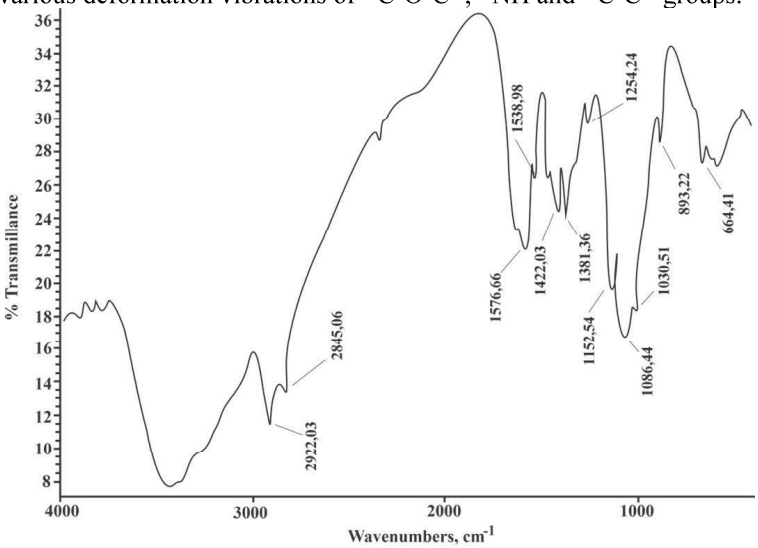

Figure 3. Fourier-transform infrared spectrum of purified *Bombyx mori* chitosan (sample No. 1, see Table 1).

3.2. Effect of the Chitosan Concentration on the Average Size of Nanoparticles

The ChS concentration is an important determinant regarding the finite size of NPs that are formed. The influence of this parameter was studied with the aim of obtaining a narrow NP size distribution and to ensure their stability in solution (Figure 4).

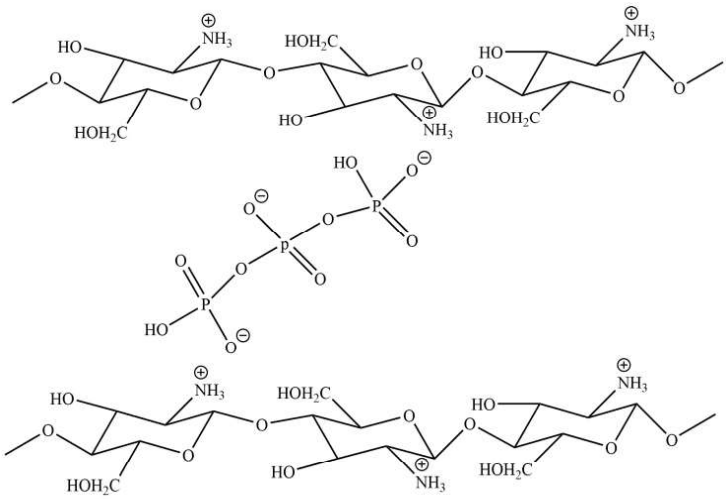

Figure 4. A schematic illustration of negatively charged sodium tripolyphosphate connecting two positively charged chitosan chains.

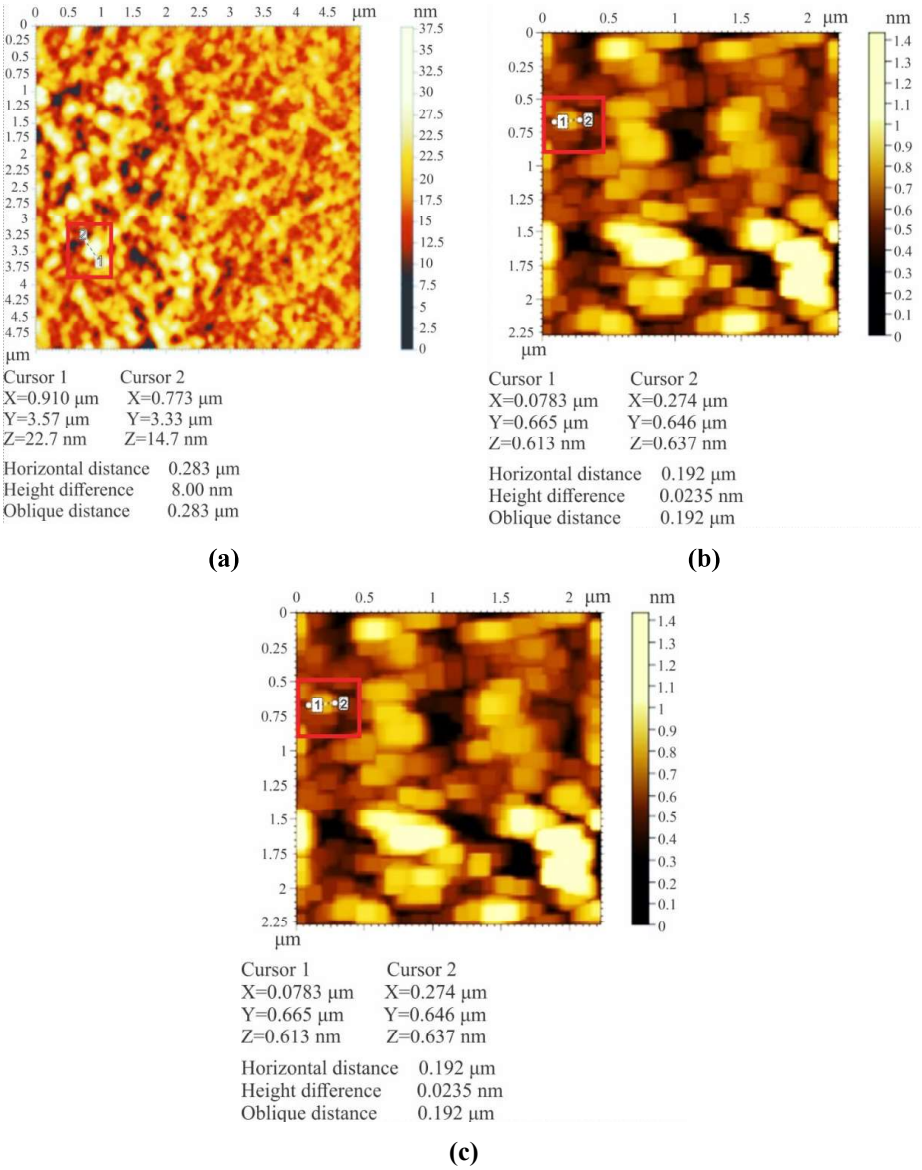

Figure 5. Atomic force micrographs of chitosan nanoparticles (ChS NPs), prepared using sample No. 1 (see Table 1): (a) 10 mg/ml ChS, 1 mg/ml sodium tripolyphosphate (TPP) and a ChS-to-TPP ratio of 1:1 yielded NPs with a size of 283 nm; (b) 1 mg/ml ChS, 1 mg/ml TPP and a ChS-to-TPP ratio of 1:1 yielded NPs with a size of 192 nm; and (c) 0.5 mg/ml ChS, 1 mg/ml TPP and a ChS-to-TPP ratio of 1:1 yielded NPs with a size of 108 nm.

AFM was performed on various samples of purified ChS. With a ChS-to-TPP ratio of 1:1, NPs were a maximum of 283, 333 and 166 nm with a ChS concentration of 10, 1 mg/ml and 0.5 mg/ml (Figure 5, Table 2). The ChS concentration greatly influenced the size of ChS NPs when studying the kinetic aspects of the size distribution of NPs

depending on the degree of nonequilibrium of the synthesis process by the method of ionotropic gelation (Table 2). When the ChS concentration increased from 0.5 mg/ml to 10 mg/ml, the size of the NPs increased from 166 to 283 nm while maintaining all other parameters of the reaction.

Consequently, a high ChS-to-TPP ratio due to a high ChS concentration corresponds to a lower cross-linking density, which ensures a slow NP formation rate and the formation of large ChS/TPP associates. This makes it possible to control the size of NPs with TPP, consistent with previous studies [26, 27].

Table 2. The dependence of the size of chitosan nanoparticles (ChS NPs) on the ChS concentration.

Figure 5 panel	ChS-to-TPP ratio	ChS concentration [mg/ml]	TPP concentration [mg/ml]	Minimum–maximum NP size [nm]
Sample No.1 (Mη = 130 kDa)				
(a)	1:1	10	1	50–283
(b)	1:1	1	1	192–333
(c)	1:1	0.5	1	108–166

Note. See Table 1 for details on sample No. 1. Abbreviation: TPP, sodium tripolyphosphate.

3.3. Effect of pH During the Production of the Average Chitosan Nanoparticle Size

Experiments were carried out with ChS with Mη = 165 kDa (sample No. 3, see Table 1) to establish how the pH of the production medium affected the ChS NP size distribution. The ChS and TPP concentrations were kept constant at 0.5 and 1 mg/ml, respectively. With a ChS solution pH of 3.8, the NPs were a maximum of 123 nm and oval in shape (Figure 6a, b, Table 3). At pH 4.1, the NPs were a maximum of 239 nm and both oval and irregularly round in shape (Figure 7a, b, Table 3). At pH 4.7, the NPs were a maximum of 388 nm (Figure 7c, Table 3). The results showed that the size of ChS NPs depends on the pH of the solution: the lower the pH of the solution, the smaller the NPs.

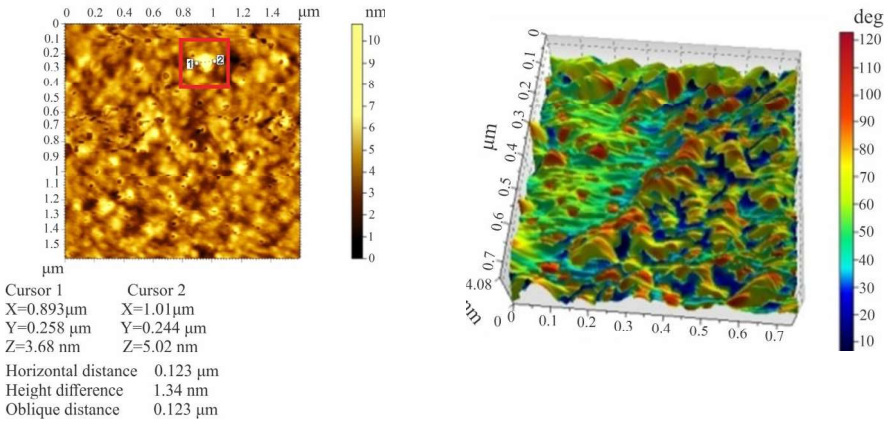

(a) **(b)**

Figure 6. (a) An atomic force micrograph of chitosan nanoparticles prepared at pH 3.8; the NPs were a maximum of 123 nm in size and oval in shape. (b) A topography image of ChS NPs formed at pH 3.8.

Table 3. The dependence of the size of chitosan nanoparticles (ChS NPs) on the pH of the solution.

No.	Sample	pH of the solution	ChS concentration [mg/ml]	Chitosan Mη [kDa]	Minimum–maximum NP size [nm]
2	NChS-1	3.8	0.5	165	1.34–123
3	NChS-2	4.1	0.5	165	1.66–239
4	NChS-3	4.7	0.5	165	0.721–388

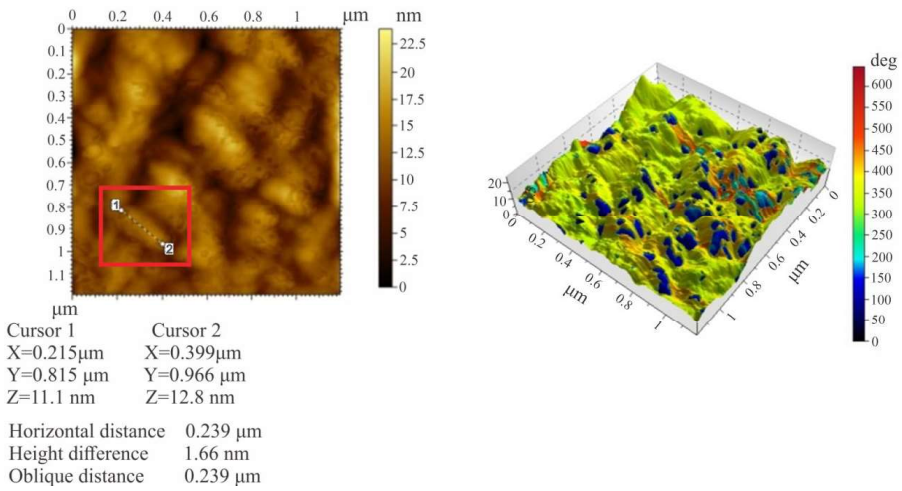

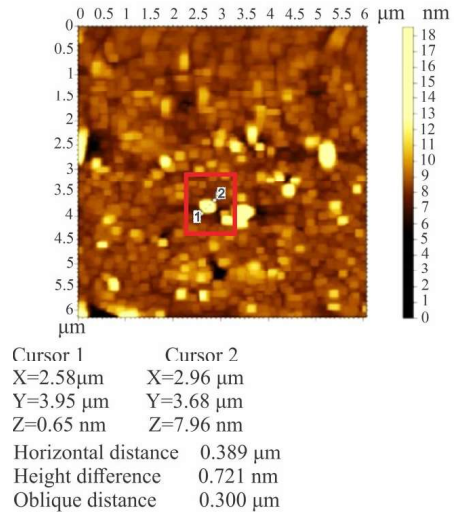

Figure 7. (a) An atomic force micrograph of chitosan nanoparticles (ChS NPs) prepared at pH 4.1; the NPs were a maximum of 239 nm in size. (b) A topography image of ChS NPs formed at pH 4.1. (c) An atomic force micrograph of chitosan nanoparticles prepared at pH 4.7; the NPs were a maximum of 388 nm in size.

3.4. Effect of Time During the Production of Chitosan Nanoparticles on the Average Size

Experiments were carried out using ChS with Mη = 152 kDa (sample No. 2, see Table 1) to determine the effect of the amount of time given to form NPs on their size. The maximum size of ChS NPs was 363 nm for a reaction time of 4 h (Figure 8a, Table 4), 564 nm for a reaction time of 8 h (Figure 8c, Table 4) and 642 nm after a reaction time of 24 h (Figure 9a, Table 4). The ChS NP formation is influenced by the reaction time. Apparently, as the synthesis time increases, it is necessary to increase the ChS-to-TPP ratio.

The mechanism of NP formation through ionic gelation has not been well described in the literature. Maintaining the stability of NPs is a very important aspect in the field of pharmaceutical nanotechnology. The NPs must be stable before use; otherwise, the therapeutic efficacy will be lost. The chemical integrity of the drug in NPs is another fundamental aspect of stability [28, 29].

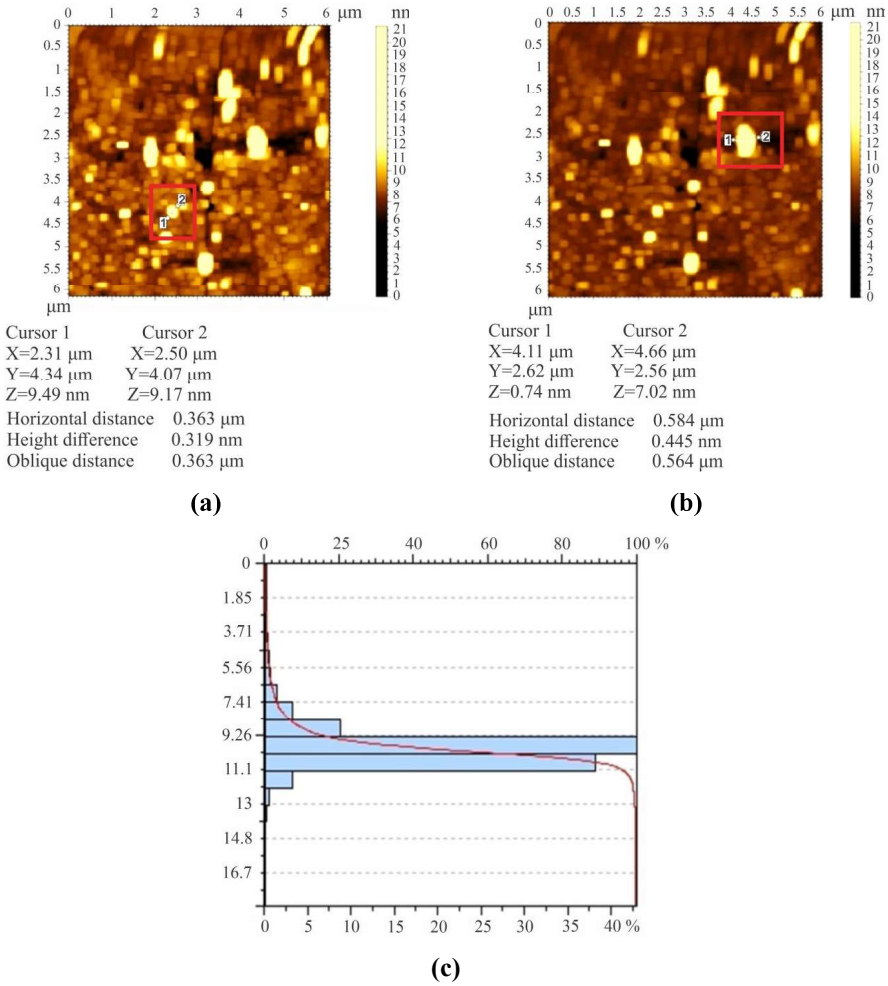

Figure 8. Atomic force micrographs of chitosan nanoparticles (ChS NPs) prepared with ChS sample No. 2 (see Table 1) with (a) a 4-h reaction time, yielding NPs with a maximum size of 363 nm, and (b) an 8-h reaction time, yielding NPs with a maximum size of 564 nm. (c) The histogram shows the NP size distribution for an 8-h reaction time.

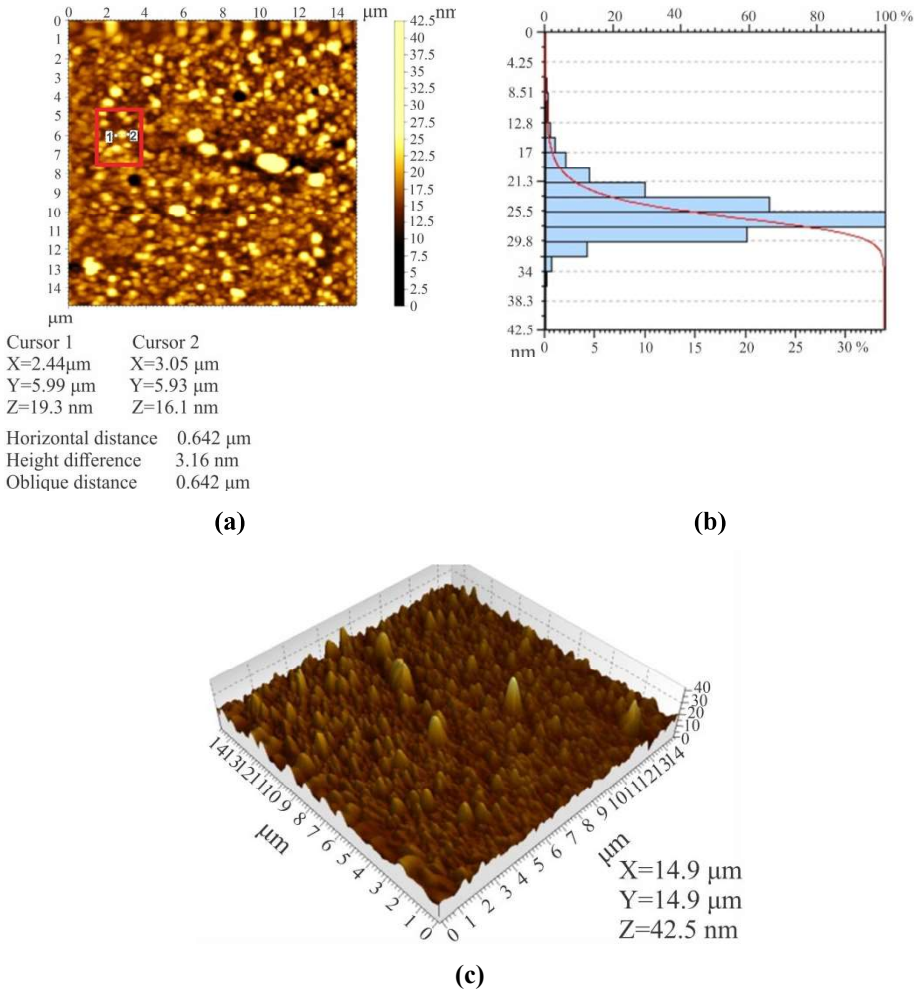

Figure 9. (a) An atomic force micrograph of chitosan nanoparticles (ChS NPs) prepared with ChS sample No. 2 (see Table 1) with a 24-h reaction time, yielding NPs with a maximum size of 642 nm. (b) The histogram shows the NP size distribution after an 24-h reaction time. (c) The surface topography of ChS NPs after a 24-h reaction time.

Table 4. The dependence of the size of chitosan nanoparticles (ChS NPs) on the reaction time.

No.	Figure	Synthesis time [h]	Ultrasound time [min]	Mη [kDa]	ChS concentration [mg/ml]	Minimum–maximum NP size [nm]
1	Figure 8a	4	2	152	0.5	319–363
2	Figure 8b	8	2	152	0.5	0.445–564
3	Figure 9a	24	2	152	0.5	3.18–642

Experimental work has shown that all ionic groups of TPP can interact with the amino groups of ChS [30–34]. Density functional theory (DFT) calculations also consider the effects of solvation, which is necessary for a correct and accurate quantitative theoretical description of the interactions that occur both during the formation of ChS and TPP NPs and their possible use as drug carriers [35–38]. In the final part of this study, we assessed on aspects of NP formation by determining interaction sites, calculating the interaction energy and searching for energetically favourable configurations between oligomers and oligomer/polyanion complexes.

3.5. Calculation Results

We obtained models of ChS/TPP systems by optimising the geometry for a variety of relative initial configurations, examining both perpendicular and parallel coordination. We focused on the possible interactions between the oxygen and phosphorus atoms of TPP and the amino and hydroxyl groups of ChS. Figure 10 shows four configurations, parallel and perpendicular (Figure 10a, b, respectively), demonstrating the strongest interactions between the completely deprotonated TPP anion ($P_3O_{10}^{5-}$) and the protonated TPP anion ($H_4P_3O_{10}^{-}$), as well as ChS chains containing protonated amino groups (–NH_3^+, Figure 10c, d).

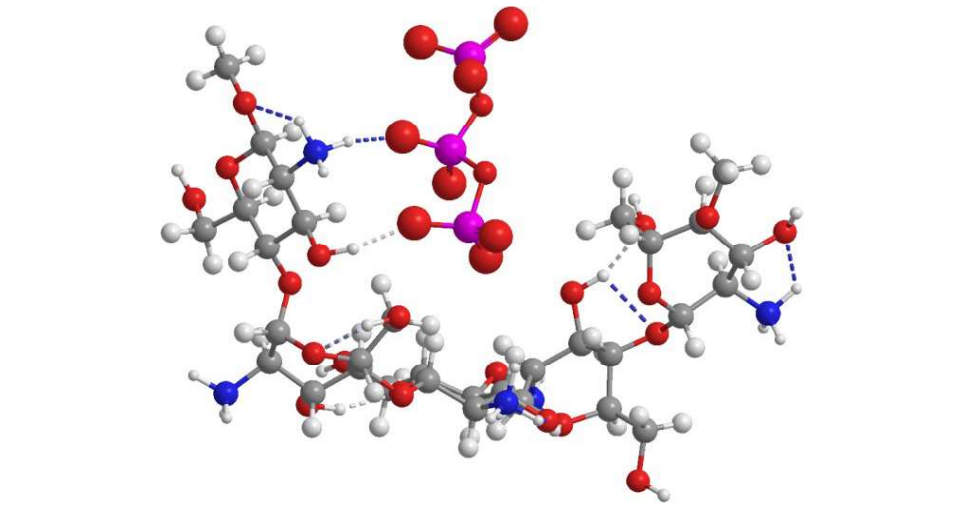

(a)

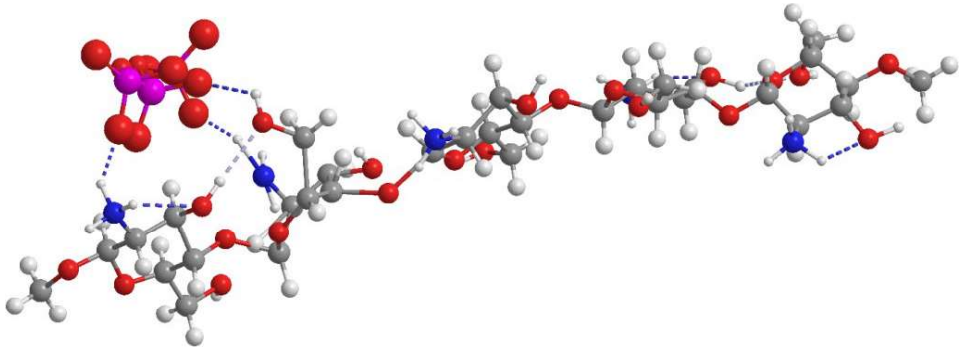

(b)

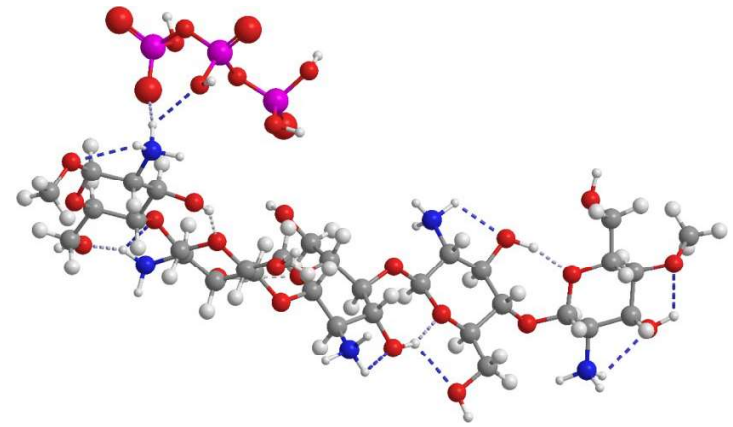

(c)

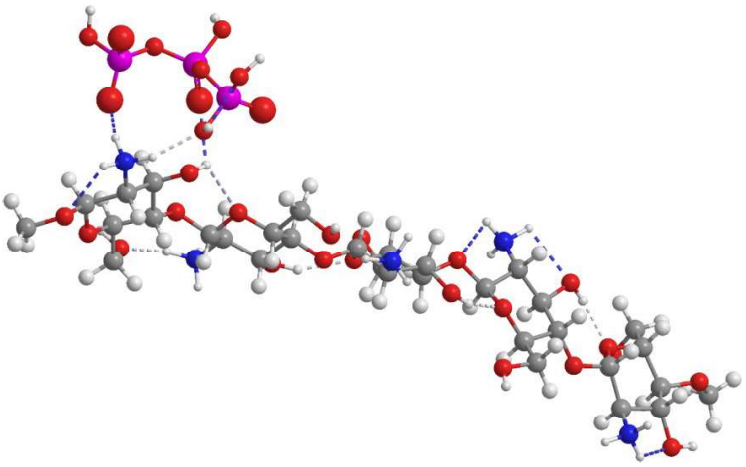

(d)

Figure 10. Calculated configurations for the interaction between the chitosan (ChS) pentamer and (a, b) deprotonated sodium tripolyphosphate (TPP, $P_3O_{10}^{5-}$) and (c, d) protonated TPP ($H_4P_3O_{10}^{-}$): (a) a parallel interaction involving one $-NH_3^+$ group and one $-CH_2OH$ group; (b) a perpendicular interaction involving two $-NH_3^+$ groups and one $-CH_2OH$, the local energy minimum with the ionic cross-linking configuration; (c) one $-NH_3^+$ group of ChS is involved in the interaction; and (d) one $-NH_3^+$ group and one $-CH_2OH$ group of ChS are involved in the interaction (both intra- and intermolecular hydrogen bonds are shown). Hydrogen atoms are white, nitrogen atoms are blue, oxygen atoms are red, carbon atoms are grey and phosphorus atoms are pink.

We calculated the interaction energy for the parallel interaction – the average distance of the TPP oxygen atoms and the ChS nitrogen atoms (two $-NH_3^+$ groups of ChS participate in the interaction) – and for the perpendicular interaction – the oxygen and phosphorus atoms of the TPP and amino and hydroxyl groups of ChS nitrogen (one $-NH_3^+$ group of ChS participates in the interaction). Figure 11 shows the change in the interaction energy as a function of the distance between the interacting atoms.

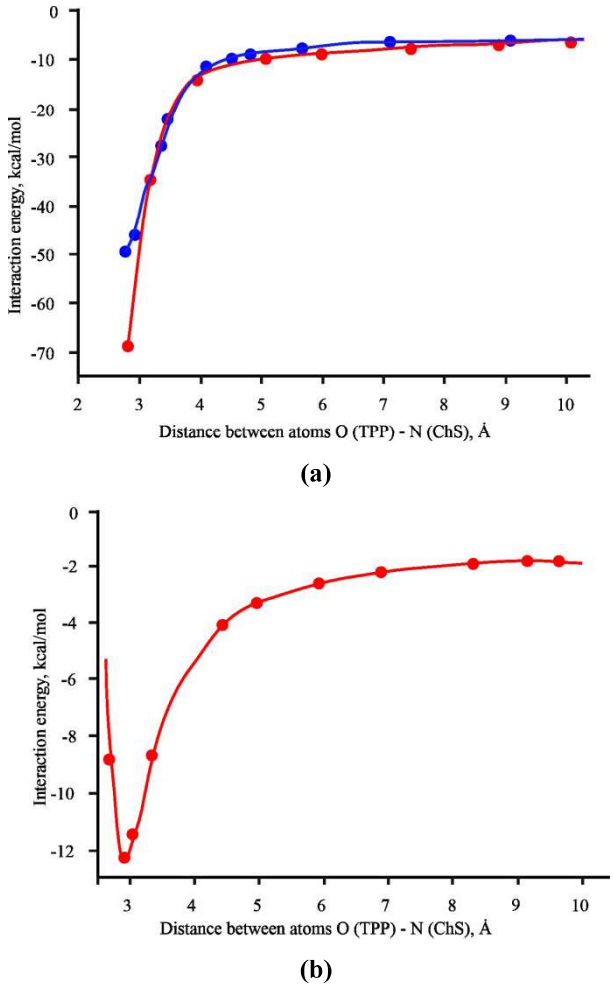

Figure 11. (a) The change in the interaction energy of the deprotonated sodium tripolyphosphate (TPP) polyanion ($P_3O_{10}^{5-}$) for the parallel approach (red line) and the perpendicular approach (blue line) on the distance between the outermost oxygen atom of TPP and the nearest nitrogen atom of ChS. (b) The change in the interaction energy of the initially protonated TPP anion ($H_4P_3O_{10}^{-}$) for the perpendicular approach depending on the distance between the interacting atoms.

We calculated the interaction energy within the framework of the gas phase model of solvation and applied BSSE corrections. We set the charge of the ChS pentamer to 5e, that is, with fully protonated amino groups. The maximum interaction energy at the local minimum of the perpendicular configuration is 50.4 kcal/mol. The interaction energy curve becomes very steep at a close distance of interacting O···N atoms of < 3.3 Å. At 2.75 Å, the transfer of a proton from the amino group of ChS to TPP reduces the interaction energy to 28.3 kcal/mol. The configuration with a global maximum interaction has a maximum interaction energy of 69.4 kcal/mol. This energy also decreases at a close distance (O···N ≈ 2.77 Å) after double proton transfer, in this case to 33.5 kcal/mol. Each of these

two proton transfers occurs between the TPP polyanion and one of the two interacting amino groups (i.e. one transfer of the proton to ChS amino group). In both cases, the drop in the interaction energy is due to proton transfer; hence, the interaction energy is significantly higher than the corresponding value in the case of a perpendicular configuration, but not twice as large as might be expected.

These findings can be explained by two facts. First, the electrostatic component of the interaction decreases unevenly during sequential proton transfer by approximately $[25-(5-n)^2]$ for the n-th proton transfer. Second, structural relaxation occurs; in this regard, the process corresponds to adiabatic proton transfer. In both cases, the final maximum interaction energy is significantly higher than what would be expected from the formation of a single O···HN hydrogen bond. In addition to the electrostatic component, a high interaction energy also results in part from long-range and weaker secondary interactions that occur between the alternative oxygen atom of TPP and the nearby hydroxyl group of ChS. We also considered the pH dependence when including the protonated TPP anion in the calculation. To do this, in addition to PES scan calculations of the deprotonated TPP anion, we also performed a similar calculation for the perpendicular approach for the protonated TPP anion ($H_4P_3O_{10}^-$; Figure 11b). In contrast to the previous calculation with the deprotonated TPP anion, the protonated TPP anion does not induce the transfer of the proton from the protonated amino group at a close range. In addition, the calculated maximum interaction energy is –12.8 kcal/mol, which is significantly lower than in the previous case, but higher than what would be expected from the formation of a single O···HN hydrogen bond [39].

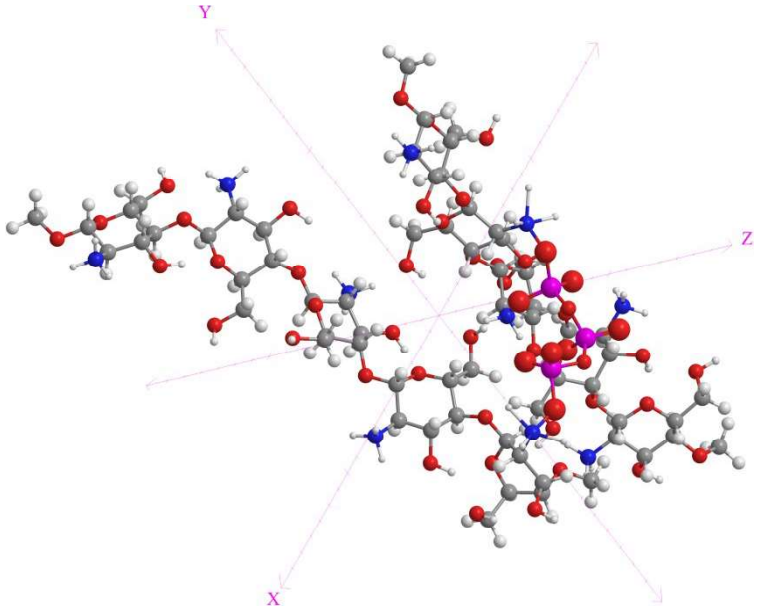

Figure 12. Cross-linked chitosan pentamers with initially deprotonated sodium tripolyphosphate.

After identifying the maximum-interaction configurations and the corresponding energies for the two TPP anions, we investigated two CS pentamers cross-linked with the deprotonated TPP anion. Although the CS oligomers are initially oriented parallel to each other, in every case their final orientation is such that the planes defined by their chain axes and the TPP primary axis form a dihedral angle of 120–135°. This situation

induces a bias in the orientation of the cross-linked CS pentamers that is expected to affect the NP formation mechanism, especially at low TPP concentrations. Figure 12 shows the optimal configuration for the ChS pentamers. The two planes correspond to a ChS chain and the TPP anion as described above; they form a dihedral angle of 127.4°

4. Conclusions

We showed that the ChS concentration (0.5–10 mg/ml) has a great influence on the size of ChS NPs when synthesised using ionotropic gelation. When the concentration increases from 0.5 to 10 mg/ml, the size increases from 100 to 300 nm while maintaining all other parameters of the reaction. Thus, an increase in the ChS-to-TPP ratio corresponds to a low cross-linking density and ensures slower kinetics of NP formation alongside the formation of large ChS/TPP associates. The pH of the medium also greatly influences the kinetics of NP formation: the size increases almost threefold, from 123 to 388 nm, when the pH increases from 3.8 to 4.7. Finally, the synthesis time also affects the size of ChS NPs: there is a slight agglomeration of NPs when increasing the time from 4 to 24 h. Apparently, with an increase in the synthesis time, it is necessary to increase the ChS-to-TPP ratio.

We performed DFT calculations to quantify the intermolecular interactions responsible for the ionic cross-linking of ChS with TPP and identified the functional groups responsible for the interaction. Based on PES scanning, the maximum interaction energy is 69.4 kcal/mol for the initially deprotonated TPP anion, decreasing to 33.5 kcal/mol after the adiabatic transfer of the proton to the protonated TPP anion. We found a maximum interaction energy of –12.8 kcal/mol for the initially protonated TPP anion. The electrostatic interaction between ChS and TPP leads to a compound that can be used to obtain NPs and surface modification of films.

5. References

[1] Barclay TG, Day CM, Petrovsky N, Garg S; (2019) Review of polysaccharide particle-based functional drug delivery. Carbohydr Polym 221, 94–112. **DOI:**10.1016/j.carbpol.2019.05.067

[2] Janes KA, Calvo P, Alonso MJ; (2001) Polysaccharide colloidal particles as delivery systems for macromolecules. Adv Drug Deliv Rev 47, 83–97. **DOI:**10.1016/s0169-409x(00)00123-x

[3] Csaba N, Garcia-Fuentes M, Alonso MJ; (2006) The performance of nanocarriers for transmucosal drug delivery. Expert Opin Drug Deliv 3, 463–478. **DOI:**10.1517/17425247.3.4.463

[4] Janes KA, Fresneau MP, Marazuela A, Fabra A, Alonso MJ; (2001) Chitosan nanoparticles as delivery systems for doxorubicin. J Control Release 73, 255–267. **DOI:**10.1016/s0168-3659(01)00294-2

[5] Pan Y, Li Y-J, Zhao H-Y, Zheng J-M, Xu H, Wei G, Hao J-s, Cui F-d; (2002) Bioadhesive polysaccharide in protein delivery system: chitosan nanoparticles improve the intestinal absorption of insulin *in vivo*. Int J Pharm 249, 139–147. **DOI:**10.1016/s0378-5173(02)00486-6

[6] Lopez-Leon T, Carvalho EL, Seijo B, Ortega-Vinuesa JL, Bastos-Gonzalez D; (2005) Physicochemical characterization of chitosan nanoparticles: electrokinetic and stability behavior. J Colloid Interface Sci 283, 344–351. **DOI:**10.1016/j.jcis.2004.08.186

[7] Koukaras EN, Papadimitriou SA, Bikiaris DN, Froudakis GE; (2012) Insight on the formation of chitosan nanoparticles through ionotropic gelation with tripolyphosphate. Mol Pharm 9, 2856–2862. **DOI:**10.1021/mp300162j

[8] Gamzazade AI, Shlimak BM, Sklyar AM, Stykova EV, Pavlova SA, Rogozin SV; (1985) Investigation of the hydrodynamic properties of chitosan solutions. Acta Polym 36, 421–424. **DOI:**10.1002/actp.1985.010360805

[9] Gosudarstvennaya farmakopeya SSSR [State Pharmacopoeia of the USSR], XI edn. 2012, Meditsina, Moscow, 24 (in Russian).

[10] Gosudarstvennaya farmakopeya SSSR [State Pharmacopoeia of the USSR], XI edn. 1987, Meditsina, Moscow, 175 (in Russian).

[11] Martynov MA, Vylegzhanina KA; (1972) Rentgenografiya polimerov: Metodicheskoe posobie dlya promyshlennykh laboratorii [Polymer X-ray spectroscopy: methodological guide for industrial laboratories]. Khimiya, Leningrad (in Russian).

[12] Klimova VA; (2001) Osnovnye mikrometody analiza organicheskikh soedinenii [Basic micromethods for the analysis of organic compounds]. Khimiya, Moscow, 75 (in Russian).

[13] Xiong Y, Feng YX, Chang M, Wang Q, Yin SN, Jian LY, Ren DF; (2023) Formulated chitosan-sodium tripolyphosphate nanoparticles for co-encapsulation of ellagic acid and anti-inflammatory peptide: characterization, stability and anti-inflammatory activity. J Sci Food Agric 103, 3447–3456. **DOI:**10.1002/jsfa.12521

[14] Maximiliano L, Agazzi M, Rovey FP, Apuzzo E, Herrera SE, Spesia MB, Mercedes de las OM, Azzaroni O; (2023) Lysozyme/tripolyphosphate complex coacervates: Properties, curcumin encapsulation and antibacterial activity. Food Hydrocoll 145, 109134. **DOI:**10.1016/j.foodhyd.2023.109134

[15] Sulaeman U, Ramadhanti SF, Diastuti H, Iswanto P, Isnaeni I, Yin S; (2023) The enhanced photo-stability of defective Ag_3PO_4 tetrahedron prepared using tripolyphosphate. Arab J Chem 161, 104409. **DOI:**10.1016/j.arabjc.2022.104409

[16] Becke AD; (1993) Density-functional thermochemistry. III. The role of exact exchange. J Chem Phys 98, 5648–5652. **DOI:**10.1063/1.464913

[17] Grimme S; (2006) Semiempirical GGA-type density functional constructed with a long-range dispersion correction. J Comput Chem 27, 1787–1799. **DOI:**10.1002/jcc.20495

[18] Schäfer A, Huber C, Ahlrichs R; (1994) Fully optimized contracted Gaussian basis sets of triple zeta valence quality for atoms Li to Kr. J Chem Phys 100, 5829–5836. **DOI:**10.1063/1.467146

[19] Miertus S, Scrocco E, Tomasi J; (1981) Electrostatic interaction of a solute with a continuum. A direct utilizaion of AB initio molecular potentials for the prevision of solvent effects. Chem Phys 55, 117–129. **DOI:**10.1016/0301-0104(81)85090-2

[20] Mennucci B; (2012) Polarizable continuum model. Wiley Interdiscip Rev Comput Mol Sci 2, 386–404. **DOI:**10.1002/wcms.1086

[21] Boys SF, Bernardi F; (1970) The calculation of small molecular interactions by the differences of separate total energies. Some procedures with reduced errors. Mol Phys 19, 553–566. **DOI:**10.1080/00268977000101561

[22] Chalasinski G, Szczesniak MM; (1994) Origins of structure and energetics of van der Waals clusters from ab initio calculations. Chem Rev 94, 1723–1765. **DOI:**10.1021/cr00031a001

[23] Galano A, Idaboy JRA; (2006) A new approach to counterpoise correction to BSSE. J Comput Chem 27, 1203–1210. **DOI:**10.1002/jcc.20438

[24] Milusheva RY, Rashidova SS; (2017) Bioactive properties of nanochitosan Bombyx mori. Polym Sci Ser C 59, 29–34. **DOI:**10.1134/S1811238217010088

[25] Muzzarelli R, Muzzarelli S; (2001) Chitosan in pharmacy and chemistry. Publishing House 'Università di Ancona', Ancona.

[26] Nasti A, Zaki NM, Leonardis Pde, Ungphaiboon S, Sansongsak P, Rimoli MG, Tirelli N; (2009) Chitosan/TPP and chitosan/TPP-hyaluronic acid nanoparticles: systematic optimisation of the preparative process and preliminary biological evaluation. Pharm Res 26, 1918–1930. **DOI:**10.1007/s11095-009-9908-0

[27] Lunkov A, Shagdarova B, Konovalova M, Zhuikova Y, Drozd N, Il'ina A, Varlamov V; (2020) Synthesis of silver nanoparticles using gallic acid-conjugated chitosan derivatives. Carbohydr Polym 15, 115916. **DOI:**10.1016/j.carbpol.2020.115916

[28] Yanat M, Schroën K; (2021) Preparation methods and applications of chitosan nanoparticles; with an outlook toward reinforcement of biodegradable packaging. React Funct Polym 161, 04849. **DOI:**10.1016/j.reactfunctpolym.2021.104849

[29] Nimesh S, Saxena A, Kumar A, Chandra R; (2012) Improved transfection efficiency of chitosan-DNA complexes employing reverse transfection. J Appl Polym Sci 124, 1771–1777. **DOI:**10.1002/app.35179

[30] Lemoine D, Francois C, Kedzierewicz F, Preat V, Hoffman M; (1996) Stability study of nanoparticles of poly (caprolactone), poly(D,L-lactide) and poly(D,L-lactidecoglycolide). Biomater 17, 2191–2197. **DOI:**10.1016/0142-9612(96)00049-X

[31] Yan Q, Li M, Dong L, Luo J, Zhong X, Shi F, Ye G, Zhao L, Fu H, Shu G, Zhao X, Zhang W, Yin H, Li Y, Tang H; (2023) Preparation, characterization and protective effect of chitosan - Tripolyphosphate encapsulated dihydromyricetin nanoparticles on acute kidney injury caused by cisplatin. Int J Biol Macromol 245, 125569. **DOI:**10.1016/j.ijbiomac.2023.125569

[32] Sawtarie N, Cai Y, Lapitsky Y; (2017) Preparation of chitosan/tripolyphosphate nanoparticles with highly tunable size and low polydispersity. Colloids Surf B 157, 110–117. **DOI:**10.1016/j.colsurfb.2017.05.055

[33] Kim ES, Baek Y, Yoo HJ, Lee JS, Lee HG; (2022) Chitosan-tripolyphosphate nanoparticles prepared by ionic gelation improve the antioxidant activities of astaxanthin in the *in vitro* and *in vivo* model. Antioxidants 11, 479. **DOI:**10.3390/antiox11030479

[34] Devi KTR, Paulraj SJ, Shah Y, Kumar SR, Kejamurthy P; (2023) Chitosan-tripolyphosphate nanoparticles encapsulated rutin targeting bacterial growth inhibition and its cytotoxicity on PANC-1 pancreatic adenocarcinoma cell. J Appl Pharm Sci 13, 141–148. **DOI:**10.7324/JAPS.2023.41561

[35] Poureghbal Y, Rahimi M, Akbari M; (2021) Ionic gelation of chitosan with sodium tripolyphosphate using a novel combined nebulizer and falling film system. Can J Chem Eng 100, 1547–1557. **DOI:**10.1002/cjce.24234

[36] Di Santo MC, D' Antoni CL, Rubio APD, Alaimo A, Pérez OE; (2021) Chitosan-tripolyphosphate nanoparticles designed to encapsulate polyphenolic compounds for biomedical and pharmaceutical applications - A review. Biomed Pharmacother 142, 111970. **DOI:**10.1016/j.biopha.2021.111970

[37] Şenol ZM, Çetinkaya S, Yenidünya AF, Başoğlu-Ünal F, Ece A; (2022) Epichlorohydrin and tripolyphosphate-crosslinked chitosan-kaolin composite for Auramine O dye removal from aqueous solutions: experimental study and DFT calculations. Int J Biol Macromol 199, 318–330. **DOI:**10.1016/j.ijbiomac.2022.01.008

[38] Moreno A, Jordana A, Grillo R, Fraceto LF, Jaime C; (2019) A study on the molecular existing interactions in nanoherbicides: a chitooligosaccharide/tripolyphosphate loaded with paraquat case. Colloids Surf A Physicochem Eng 562, 220–228 **DOI:**10.1016/j.colsurfa.2018.11.033

[39] Řezać J, Riley KE, Hobza P; (2011) S66: a well-balanced database of benchmark interaction energies relevant to biomolecular structures. J Chem Theory Comput 7, 2427–2438. **DOI:**10.1021/ct2002946